EURISOL DS Project

EURISOL DS Project
Task 11: Beam intensity calculation

Deliverable D2
Fragmentation of post accelerator ISOL beams
Report of optimal post-acceleration energy

Planned Date (month): 33

Achieved Date (month): 48

Lead Contractor(s): USDC

Project acronym: *EURISOL DS*

Project full title: *EUROPEAN ISOTOPE SEPARATION ON-LINE*

RADIOACTIVE ION BEAM FACILITY

Start of the Project: *1st February 2005*

Duration of the project: *54 months*

Fragmentation of post accelerator ISOL beams

In the course of the intense discussion on the design of future secondary-beam facilities, different scenarios for the production of secondary beams have been introduced. In particular, numerous ideas have been developed, which exploit specific aspects of nuclear reactions and technical solutions, e.g. with respect to limitations on heat load, ISOL efficiencies or background intensities. The most severe limitations are given by the difficulties to extract the refractory elements from the target. A possibility to overcome this problem could be a two-step reaction mechanism [1] – In the first step an intense beam of a neutron-rich ISOL beam is produced. This beam is then accelerated and fragmented in a secondary target, and with a help of a magnetic separator the wanted secondary beam is selected. Since the projectile-fragmentation process is not subject to the restrictions of the ISOL method, also refractory elements can be produced in this way. Another advantage of this approach could be that two reaction processes, fission of a neutron-rich actinide and cold fragmentation of a neutron-rich fission are combined, which might allow producing extremely neutron-rich isotopes not reachable by fission only.

Important aspect of this approach is of course the suited energy of the post-accelerator. Different aspects, e.g. reaction mechanism, charge-state distributions or optimal target thickness, have to be considered in order to decide on the optimal *energy of the post-accelerator*. These questions are discussed in the following sections.

Up to now, there were no data available on the nuclide production by fragmentation of extremely neutron-rich fission fragments, and therefore the benefit of this approach could have only be estimated by model calculations only. These data have been measured in the frame of Subtask 2 (projectile energies above 100·A MeV) and Subtask 6 (projectile energies ~ 30·A MeV), and will be used as a basis for quantitative estimate on the fragmentation of a post-accelerated ^{132}Sn beam and the optimal energy of the post-accelerator. This should be the most favourable case for this approach, because it populates neutron-rich isotopes of the refractive elements between Zr and Pd, which cannot be extracted at all from the

RIDS 515768	TASK: 11	DATE:	
DELIVERABLE: D2		PAGE 2	

ISOL target with present technology.

I. Nuclear-reaction aspects

The character of heavy-ion reactions changes as a function of projectile velocity. While for energies close to the Coulomb barrier the nuclear potential is decisive, favouring fusion reactions, at least for the lower angular momenta, for beam velocities exceeding the Fermi velocity it is the abrasion picture which governs the nuclear collision. The transition region, about $20 \cdot A$ MeV to $30 \cdot A$ MeV is characterized by incomplete-fusion reactions and a considerable nucleon exchange between projectile and target. It is expected that energies around $50 \cdot A$ MeV to $100 \cdot A$ MeV are sufficient for the abrasion picture to be dominant. With the reservation of more elaborate investigations, it seems reasonable to assume that the reaction mechanism does not substantially change in the energy range above $50 \cdot A$ MeV.

I.1 Projectile energies above 100 AMeV

I.1.1 Experimental set-up and data analysis

The experiment was performed at the GSI facilities in Darmstadt. There the synchrotron SIS18 was used to accelerate a ^{238}U beam at $950 \cdot A$ MeV. The beam was then conducted until the FRagment Separator (FRS) [2] experimental area. There the beam impinged onto a 650 mg/cm^2 lead target inducing the fission of the ^{238}U projectiles. Fission fragments flying forward entered into the zero-degree magnetic spectrometer FRS. A second 2600 mg/cm^2 beryllium target placed at the intermediate image plane of the spectrometer was used for inducing the fragmentation of the neutron-rich fission fragments transmitted until that point of the spectrometer. Both sections of the FRS were equipped with specific detectors providing the full isotopic identification of the fission fragments (first section) and their fragmentation residues produced in the beryllium target (second section).

Time-projection chambers (TPC in Fig.1) placed at the intermediate (F2) and final (F4) image planes and two time-of-flight measurements (ToF1 and ToF2) using plastic scintillators (SCI1, SCI2 and SCI4) provided the $B\rho$ and velocity determination of the transmitted nuclei in both sections of the spectrometer. Then, two fast ionisation chambers placed also at the end of both sections provided an energy-loss measurement used for the determination of the atomic number of the fragments. Details on the data

RIDS 515768	TASK: 11	DATE:	
DELIVERABLE: D2		PAGE 3	

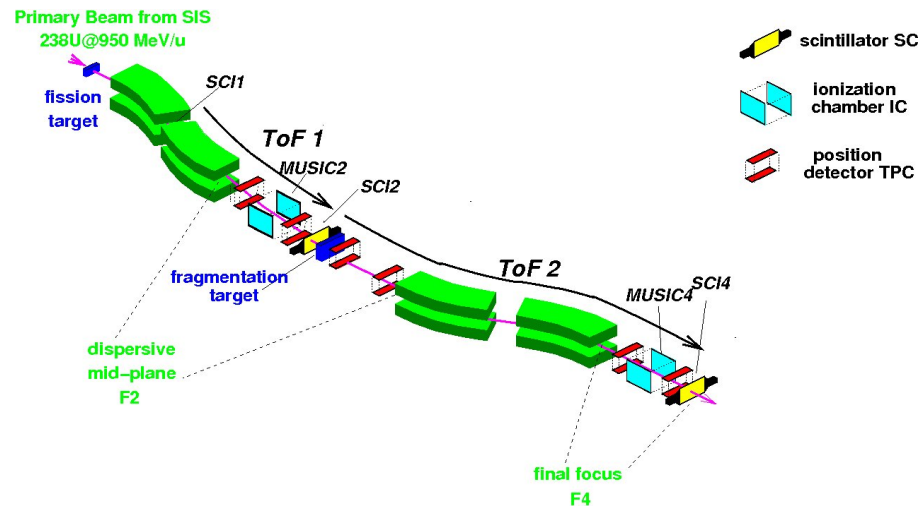sorting for similar experiments can be found in references [2,3,4].

Figure 1. Schematic layout of the FRS showing the dipole magnetic elements and the detection system used in the experiment.

Several challenges were faced in this experiment although the most critical one was the identification of the fission fragments in the first section of the FRS. In this case, and in order to avoid the primary beam, the time-of-flight measurement was done using plastic scintillators behind the first and second dipoles of the FRS with a limited flight path around 20 m (see Fig. 1). These plastic scintillators where equipped with fast photomultiplier H2431-50MOD from Hamamatsu accepting a counting rate at the first image plane of the spectrometer (SCI1 in Fig. 1) up to 250 kHz and providing a time resolution as good as 72 ps, enabling the determination of the mass number of the fission fragments at the intermediate image plane with a resolution of $\Delta A/A \sim 1.4 \cdot 10^{-3}$. In the second section of the FRS the measurement of the time-of-flight could be done using a larger flight path (~36 m) providing then an even better mass resolution ($\Delta A/A \sim 1 \cdot 10^{-3}$).

In Fig. 2 we report two typical identification matrices obtained with the detectors placed along the first (left panel) and second (right panel) sections of the FRS for a magnetic tuning centred around ^{132}Sn in the fist section and ^{131}In in the second section. The identification matrix in the second section is obtained under the condition that ^{132}Sn is identified in the first section of the FRS, showing then not only the not reacting ^{132}Sn nuclei but also some of its fragmentation residues as the one (^{131}In) and two (^{130}Cd) proton

removal channels. As can be seen, the resolution obtained in both measurements is more than enough in order to provide an unambiguous separation and identification of the fission fragments and their subsequent fragmentation residues.
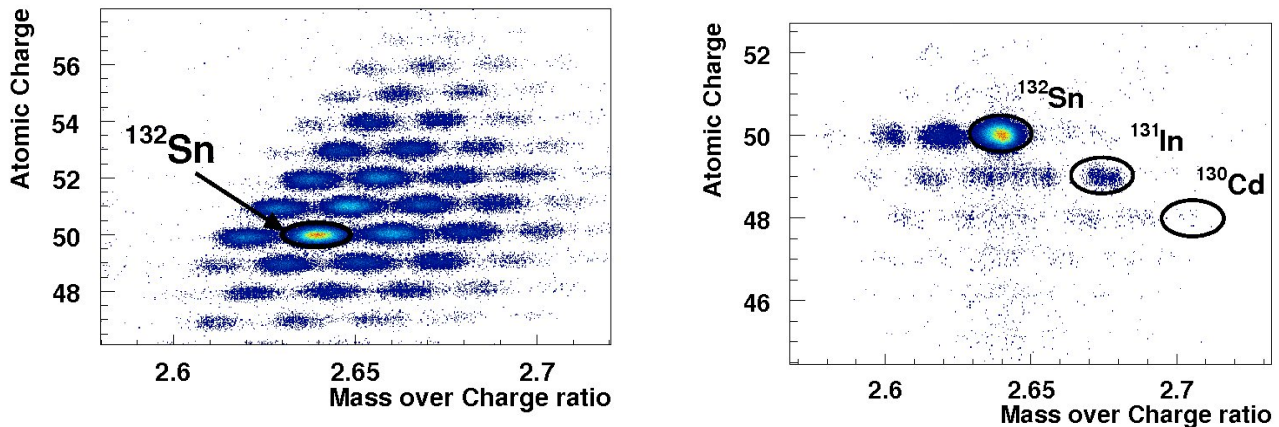

Figure 2. Left panel: two-dimensional scatter plot of the fission fragments energy loss versus their *A/Q* value isotopically identified in the first section of the FRS. The ^{132}Sn is indicated. Right panel: Identification matrix of the fragmentation residues of ^{132}Sn at the final focal plane of the FRS. ^{132}Sn and the one-proton (^{131}In) and two-proton (^{130}Cd) removal channels are indicated.

I.1.2 Production cross sections

In order to determine the production of the most neutron-rich residual nuclei issued in the fragmentation of ^{132}Sn in beryllium with cross sections larger than 10 µb several magnetic tunings of the second section of the FRS centred on ^{132}Sb, ^{132}Sn, ^{131}In, ^{129}Ag, ^{126}Ag and ^{123}Ag were required. The lower cross section limit reached in this measurement was determined by the rate of ^{132}Sn nuclei transmitted until the intermediate image plane of the FRS (~ 1000 s^{-1}) and a reasonable time for the measurement (2 days for the most exotic tuning). Nevertheless, the main limitation for the experiment was not the primary beam intensity, in our case restricted to 10^8 ^{238}U s^{-1}, but the high number of contaminants reaching the intermediate image plane of the FRS (other fission residues) together with an acquisition rate limited to few kHz.

For normalization purposes we used two triggers in this experiment, a fission beam trigger provided by the scintillator placed at the intermediate image plane of the FRS (SCI2), scaled down by a constant factor in order to keep an acquisition dead time below 30%, and a fragmentation trigger given by the

The fragmentation yields measured at the final image plane of the FRS under the condition that a ^{132}Sn nucleus reached the intermediate image plane, was corrected by the probability for multiple reactions and the ^{132}Sn intensity attenuation in the beryllium target, secondary reactions in all other layers of matter traversed by the fragmentation residues determined from a measurement without beryllium target, optical transmission between the intermediate and final image planes of the FRS and the acquisition dead time. These yields were then normalised to the target thickness and the number of ^{132}Sn reaching the intermediate image plane of the FRS corrected by the trigger scaling down parameter.

The measured production cross sections of residual nuclei issued in the fragmentation of ^{132}Sn projectiles are depicted in Fig. 3. As can be seen, very neutron-rich isotopes of In, Cd, Ag, Pd, Rh and Ru with cross sections as low as 10 μb were produced covering the gap of refractory elements in this region of the chart of the nuclides. In the case of In, Cd and Ag we reached the most neutron-rich nuclei that can be produced in the fragmentation of ^{132}Sn corresponding to the one (^{131}In), two (^{130}Cs) and three (^{129}Ag) proton removal channels. Error bars are dominated by statistical uncertainties.
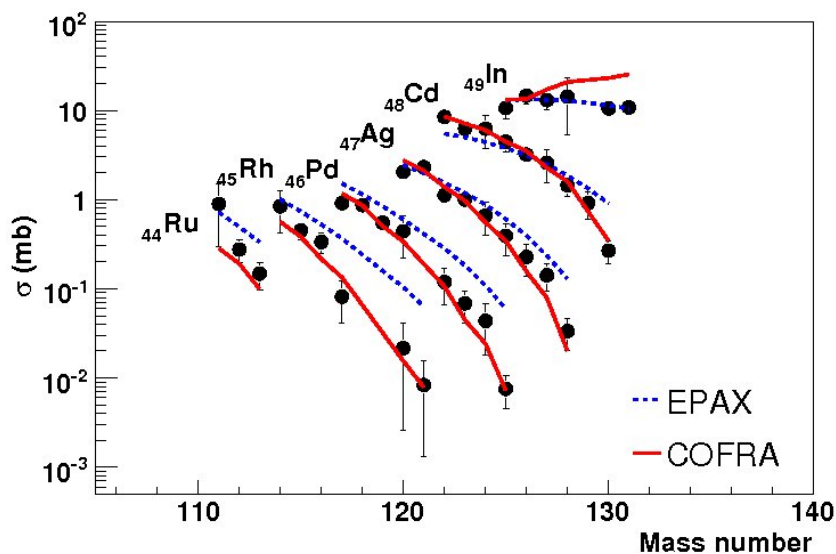

Figure 3. Isotopic distributions of the production cross sections of residual nuclei issued in the fragmentation of ^{132}Sn projectiles in beryllium.

I.1.3. Benchmarking of model calculations

The production of the most neutron-rich residues in fragmentation reactions is expected by the cold-fragmentation process [6]. These are reaction channels where the projectile nucleus mostly loses protons in the interaction with the target and, at the same time, deposits only little excitation energy, allowing for the evaporation of a few neutrons. Obviously, the production of the most neutron-rich final residues relies on large fluctuations in the proton-to-neutron ratio of the abraded nucleons and in the excitation energy gained by the projectile pre-fragment in the abrasion process. The case we are investigating provides an excellent example for investigating these fluctuations since the binding energy of our projectile and fragmentation residues is smaller compared to the case of stable projectiles. In this scenario, the most extreme case corresponds to the proton-removal channels where only protons are abraded and the excitation energy gained remains below the neutron-evaporation threshold. As already mentioned in the previous section, in this experiment we were able to identify and measure the production cross sections up to the three proton-removal channel.

The future perspectives for the production of medium-mass neutron-rich nuclei using the fragmentation of ^{132}Sn projectiles at the future EURISOL facility can be investigated using model calculations validated by the present data. For this purpose we chose two different approaches. The EPAX formula [7], a semi-empirical parametrisation of previously measured data and the code COFRA [6] a simplified version of the abrasion-ablation model ABRABLA [8]. COFRA includes a complete description of the abrasion process following the ideas introduced by Gaimard and Schmidt [8] with a reduction of the excitation energy by 10% with respect to the description proposed in Ref. [9]. Then the evaporation stage is based on the statistical model using the Weisskopf prescription but considering only neutron emission as open de-excitation channel. This simplification allows for an analytical description of the evaporation process as described in [6] but restricts the validity of the results to those cases where the de-excitation of an excited nucleus can be described mostly by the evaporation of neutrons, as it is the case of nuclei with a large neutron excess, and in particular, those produced in cold-fragmentation reactions.

In Fig. 3 we compare the results obtained with both calculations with the data measured in the present work. The EPAX formula in general provides a good description of the production cross sections of neutron-deficient fragmentation residues [10]. In the present case, EPAX describes rather well the production cross sections of residual nuclei not too different in mass number from the projectile. However, for residual nuclei with a large neutron excess EPAX clearly overestimates the production

RIDS 515768 TASK: 11	DATE:	
DELIVERABLE: D2	PAGE 7	

cross sections. This effect increases with the difference in mass number between the residual nucleus and the projectile, being close to one order of magnitude already for the three proton-removal channel shown in Fig. 3. This overestimation of the production cross sections of residual nuclei with large neutron excess and far from the projectile obtained with EPAX was already observed in previous works [1,6,11,12].

The code COFRA provides a better overall description of the present data. Nevertheless, we can also identify a clear tendency to slightly under-predict the production cross sections of neutron-rich residual nuclei with a large difference in mass number with respect to the projectile, as can be seen in Fig. 3. It should be stressed that the predictions of the COFRA code are extremely sensitive to the precise values of the neutron separation energies of the nuclei of interest. Indeed, an overestimation of few hundred keV in the neutron binding energies could explain the observed deviations from the measured cross section.

I.1.4. Energy dependence of the fragmentation cross sections

The energy dependence of the production cross sections of residual nuclei in fragmentation reactions was investigated using data previously obtained for the reaction ^{136}Xe+Ti at 1000·A MeV, 500·A MeV and 200·A MeV shown in Fig. 4. As can be seen in this figure, some of the isotopic distributions of residual nuclei produced in peripheral collisions show a clear dependence with the energy. In particular for residual nuclei close in mass number to the projectile, e.g. xenon and indium isotopes, the final cross sections increase inversely with the energy of the projectile. Lighter residual nuclei, e.g. tin isotopes follow the expected energy independence.

A detailed analysis performed in task 11.4 allowed us to conclude that the observed dependence with the energy of the production cross sections of residual nuclei close in mass to the projectile can be explained as due to charge exchange channels. This effect is particularly visible for residual nuclei close in mass to the projectile where the difference in production cross section between consecutive elements is rather small. For lighter residues, the difference in production cross section between a given element Z and the following one Z-1 is large enough to consider as negligible the contribution of the charge exchange channels. This effect also reduces with energy since the probability for the charge exchange decreases at higher projectile energies.

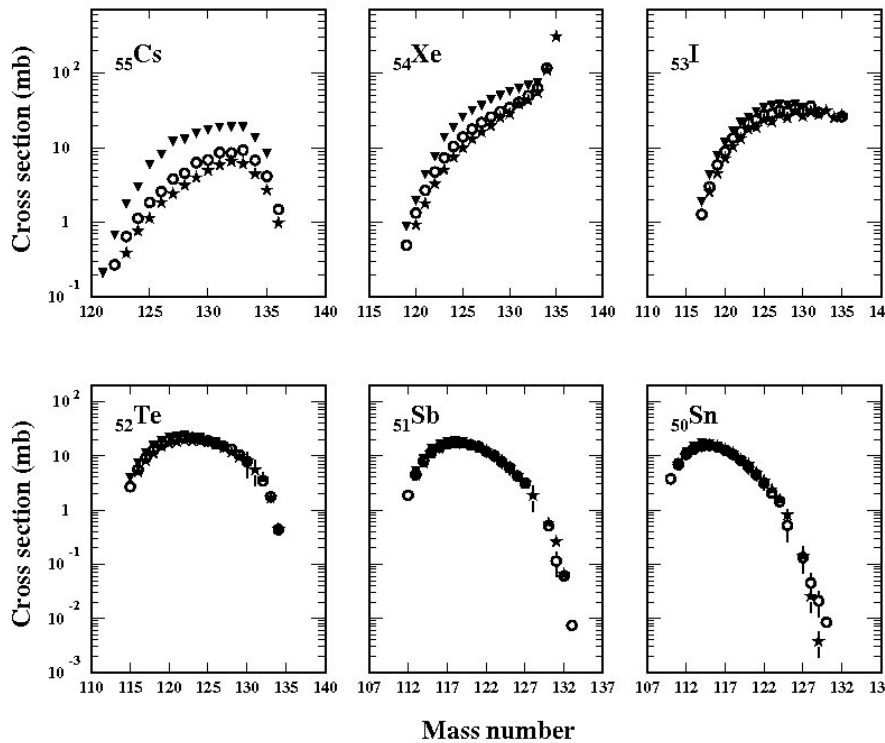| RIDS 515768 TASK: 11	DATE:	
DELIVERABLE: D2	PAGE 8	

Figure 4: Isotopic distributions of the production cross sections of residual nuclei produced in projectile fragmentation reactions induced by ^{136}Xe projectiles impinging a titanium target at 1000·A MeV (stars), 500·A MeV (circles) and 200·A MeV (triangles).

We can then conclude that the observed effect could be relevant only for the production neutron-deficient isotopes of elements close to the projectile. The production of neutron-rich nuclei is not affected by the charge exchange reactions being thus independent on the initial projectile energy down to 200·A MeV as shown in this work. Evidences from other works indicate that this lower limit could be between 100·A MeV and 150·A MeV.

I.1.5. Estimated productions at EURISOL

In order to estimate the expected production yields in a two-step scenario at Eurisol we must use not only

the measured cross sections in this work but also some assumptions on the productions in the primary target. The numbers we use are the following: A total fission rate of 10^{16} s^{-1} in the high-power target, leading to an in-target production of ^{132}Sn of about 10^{14} s^{-1}. This production will be reduced by the target release, ionisation and acceleration efficiencies to about 10%, being the expected intensity of re-accelerated ^{132}Sn of 10^{13} s^{-1}. Considering a beam energy of 120·A MeV, the optimum thickness for the beryllium fragmentation target would be 400 mg/cm2, which corresponds to about 50% of the range of the ^{132}Sn in beryllium and a 6.5% reaction probability. For a nucleus, which is produced with a cross section of 1 mb, the conversion rate in this target amounts to $2.7 \cdot 10^8$ s^{-1}. The expected intensities obtained by fragmentation of the re-accelerated ^{132}Sn are depicted in Fig. 5. The cross sections were calculated with the COFRA code. We have chosen this code in order to obtain a conservative estimate, because as discussed in the previous section, it gives more realistic estimates on the production cross sections of neutron-rich nuclei.
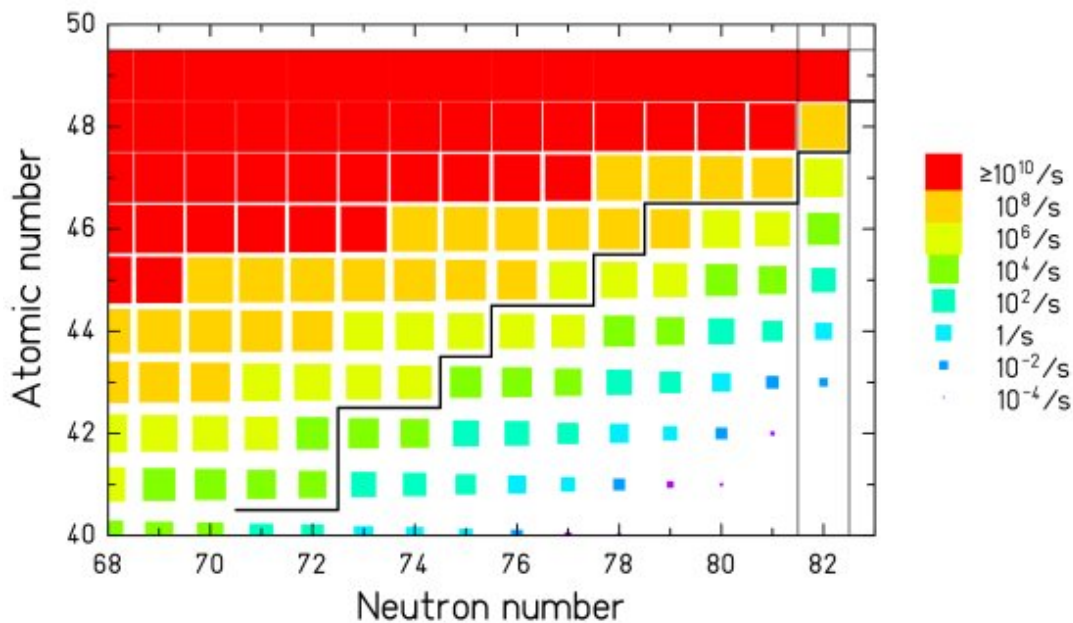

Figure 5: Intensities obtained in EURISOL by fragmentation of a ^{132}Sn beam calculated with the COFRA code. The ^{132}Sn is assumed to have an energy of 120·A MeV and an intensity of $2 \cdot 10^{13}$/s. The stair function denotes the limit of known nuclides.

As can be seen in Fig. 5, the fragmentation of intense beams of ^{132}Sn not only covers the region of refractory elements unreachable to ISOL-type facilities but also makes it possible to extend considerably

the present limits of the chart of the nuclides. The present calculations show that this techique will open the possibility for nuclear structure investigations of extremely neutron-rich nuclei with an atomic number down to six units below the one of the projectile. This technique can also be applied with other fission residues having large extraction efficiencies from the ISOL target. The combination of few selected fission residues as fragmentation projectiles will make possible the production of a large variety of medium-mass neutron-rich nuclei. Detailed calculations using the tools developed or benchmarked in this work could provide the expected productions for all nuclei accesible with this technique.

I.1.6. Production yields in ^{136}Xe and ^{132}Sn fragmentation

The competitivity of the two-step reaction scheme in ISOL-type facilities in producing medium-mass neutron-rich nuclei can be demonstrated by comparing the measured production cross sections in this work with the expected production in typical fragmentation reactions induced by stable projectiles used in in-flight facilities. For this purpose we use the measured production cross sections of residual nuclei in fragmentation reaction induced by ^{136}Xe projectiles impinging into a beryllium target presented in Ref. [12].

In Fig. 6 we report the measured cross sections of the proton-removal channels in reactions induced by ^{136}Xe and ^{132}Sn projectiles in a beryllium target around $1000 \cdot A$ MeV. The proton-removal channels correspond to the most neutron-rich nuclei that can be produced in fragmentation reactions. In the two reactions investigated the proton-removal channels are located along the N=82 line. In both cases the measured cross sections are compared to predictions obtained with the code COFRA. As already discussed in previous sections, these predictions describe quite accurately the experimental results. However, the EPAX parameterization overestimates the data.

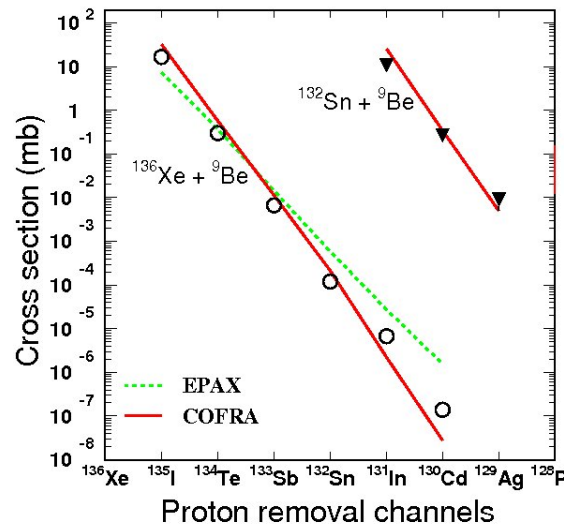**Figure 6**. Production cross sections of the proton-removal channels in the reactions ^{136}Xe+Be and ^{132}Sn+Be around 1000·A MeV. The data points are compared to the predictions obtained with two approaches, the COFRA model (solid line) and the EPAX formula (dashed line).

The comparison of the final cross sections in both reactions clearly shows that in average, the production of a given nucleus has a cross sections around six orders of magnitude higher in cold-fragmentation reactions induced by ^{132}Sn projectiles than in the case of ^{136}Xe projectiles. The final yields will also depend on the respective primary beam intensities and target thicknesses. Future in-flight facilities like FAIR are expected to produced beams of heavy ions, in particular ^{136}Xe, with an intensity up to 10^{12} ions s^{-1}. As we have seen in the previous section, the high power target at the future Eurisol facility is expected to produce up to 10^{16} fissions per second, and therefore some 10^{14} nuclei of ^{132}Sn per second. Assuming an overall release, ionization and acceleration efficiency around 10 %, the expected intensity of an ^{132}Sn beam would be at least of the same order of a ^{136}Xe beam in an in-flight facility $\sim10^{12}$ ions s^{-1}. Taking into account that fragmentation targets in the two-step scheme are around one order of magnitude thinner than the ones that can be used in in-flight facilities, Eurisol would still provide final yields of medium-mass neutron-rich nuclei with an intensity up to five orders of magnitude higher than in an in-flight facility. Moreover, the possibility of using the two-step technique with other fission residues will give access to a larger number of extremely neutron-rich nuclei in the medium-mass region of the chart of the nuclides.

I.2. Projectile energies up to 30 AMeV

In the Fermi-energy regime, production of neutron-rich nuclides in heavy-ion reactions is related to nucleon exchange between target and projectile. While at energies above ~ 100·A MeV neutron excess of the target does not have influence on the N/Z ratio of reaction product, in the Fermi-energy regime by a suitable choice of the target nucleus one can enhance the production of neutron-rich nuclei. An open question in this regime is the optimum energy of the initial beam, and thus the earlier high-resolution data at 25·A MeV [13] was supplemented by experimental data of comparable quality at lower beam energy 15·A MeV, which can be beneficial for neutron-rich products due to lower excitation energy and longer reaction time.

1.2.1 Experimental set-up

The study was performed at the Cyclotron Institute of Texas A&M University. A 15·A MeV ^{40}Ar and ^{86}Kr beams from the K500 superconducting cyclotron, with a typical current up to 10 pnA, interacted with ^{27}Al and ^{58,64}Ni targets of typical thickness around 2.0 mg/cm2. The reaction products were analyzed with the MARS recoil separator [14]. The primary beam struck the target at 4 degrees relative to the optical axis of the spectrometer. The direct beam was collected in a small square Faraday cup. The fragments were accepted in the angular opening of MARS, in this setting in the range 2.0—6.0 degrees (the angular acceptance of MARS is 9 msr). MARS optics provides one intermediate dispersive image and a final achromatic image (focal plane) and offers a momentum acceptance of 4 %.

At the focal plane, the fragments were collected in a ΔE-E Si detector telescope. The ΔE detector was a large area Si strip detector of 65 μm thickness, whereas the E detector was a single-element Si detector of 950 μm. Time of flight was measured between two parallel plate avalanche counters (PPACs) positioned at the dispersive image and at the focal plane, respectively, and separated by a distance of 13.2 m. The PPAC at the dispersive image was also X-Y position sensitive and used to record the position of the reaction products. The horizontal position, along with NMR measurements of the field of the MARS first dipole, was used to determine the magnetic rigidity $B\rho$ of the particles.

Thus, the reaction products were characterized by an event-by-event measurement of the energy loss, residual energy, time of flight, and magnetic rigidity. The response of the spectrometer and detector system to ions of known atomic number Z, mass number A, ionic charge q and velocity was calibrated using low intensity primary beams. To cover the N/Z and velocity range of the fragments, a series of measurements was performed at overlapping magnetic rigidity settings in the range 1.1-1.5 Tm.

The determination of the atomic number Z was based on the energy loss of the particles in the first ΔE detector and their velocity, with a resulting resolution (FWHM) of 0.6 Z units for $A<90$. The ionic charge q of the particles entering the spectrometer after the Al stripper, was obtained from the total energy, the velocity and the magnetic rigidity [13]. The measurement of the ionic charge q had a resolution of 0.5 q units (FWHM) for $A<90$. Since the ionic charge must be an integer, we assigned integer values of q for each event by putting appropriate windows on each peak of the q spectrum at each magnetic-rigidity setting of the spectrometer. Using the magnetic rigidity and velocity measurement, the mass-to-charge A/q ratio of each ion was obtained and combining the q determination with the A/q measurement, the mass A was obtained.

Combination and appropriate normalization of the data at various magnetic rigidity settings of the spectrometer provided fragment distributions with respect to Z, A, q and velocity. Correction of missing yields caused by charge changing at the PPAC (positioned at the dispersive image) was performed. The isotope distributions were subsequently summed over all values of q. Thus the resulting distributions in Z, A and velocity are the fragment yield distributions measured in the angle interval 2.0-6.0 degrees and in the magnetic rigidity range 1.1-1.5 Tm.

I.2.2. Production cross sections

Numerical values and comparison with model calculations

Figure 7 presents the mass yield curve from the reaction $^{40}Ar+^{27}Al$ at 15·A MeV at 4 degrees. The measured data, normalized for beam current and target thickness are given in mb and presented as solid squares. The result of the PE+DIT/ICF+SMM calculation [15,16,17] filtered by the spectrometer angular, azimuthal and momentum acceptance is given by the full line. A comparison of the measured yields to the calculated filtered yields shows reasonable overall agreement for the projectile-like nuclei with Z=11-19. The discrepancies at the proton-rich side can be caused by experimental ($B\rho$) limitations while for the

three lightest elements similar limitations appear to be exhibited also on the neutron-rich side. In general one can consider that at 15·A MeV the PE+DIT/ICF+SMM simulation appears to be equally successful as at the energy 25·A MeV.
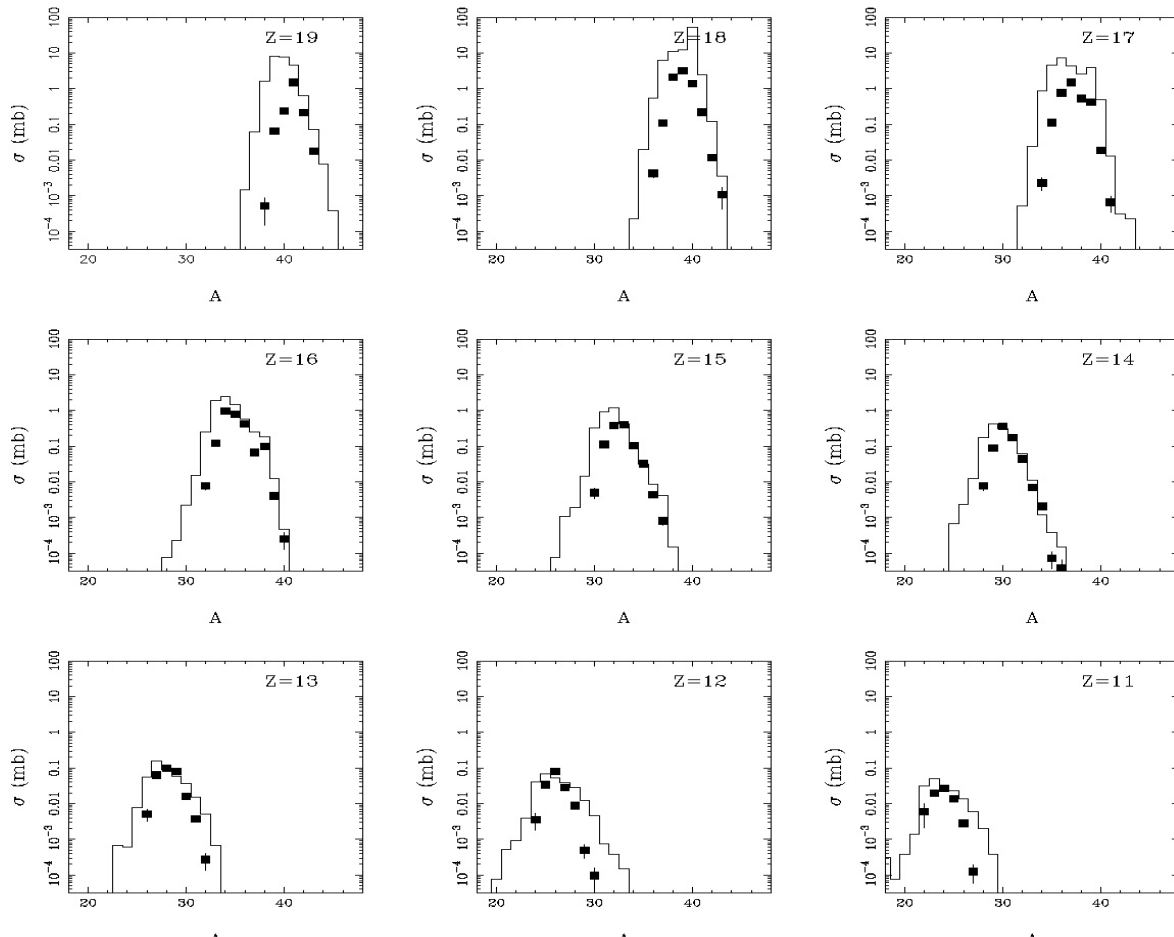

Figure 7: Mass yield curves from the reaction ^{40}Ar+^{27}Al at 15·A MeV at 4 degrees. Solid squares - measured data. Lines - result of the PE+DIT/ICF+SMM calculation [15,16,17], filtered by the spectrometer angular, azimuthal and momentum acceptance.

This conclusion is supported also by the mass yield curve from the reaction ^{40}Ar+^{64}Ni at 15·A MeV at 4 degrees shown in Fig. 8. Also in this reaction the PE+DIT/ICF+SMM shows similarly successful as in the previous case. The apparent lack of the calculated yields for the three lightest elements can stem from more forward focused angular distributions of these products originating from ICF collisions, suggesting

lower azimuthal factors than the ones used which were obtained assuming even spread of products over spectrometer coverage.

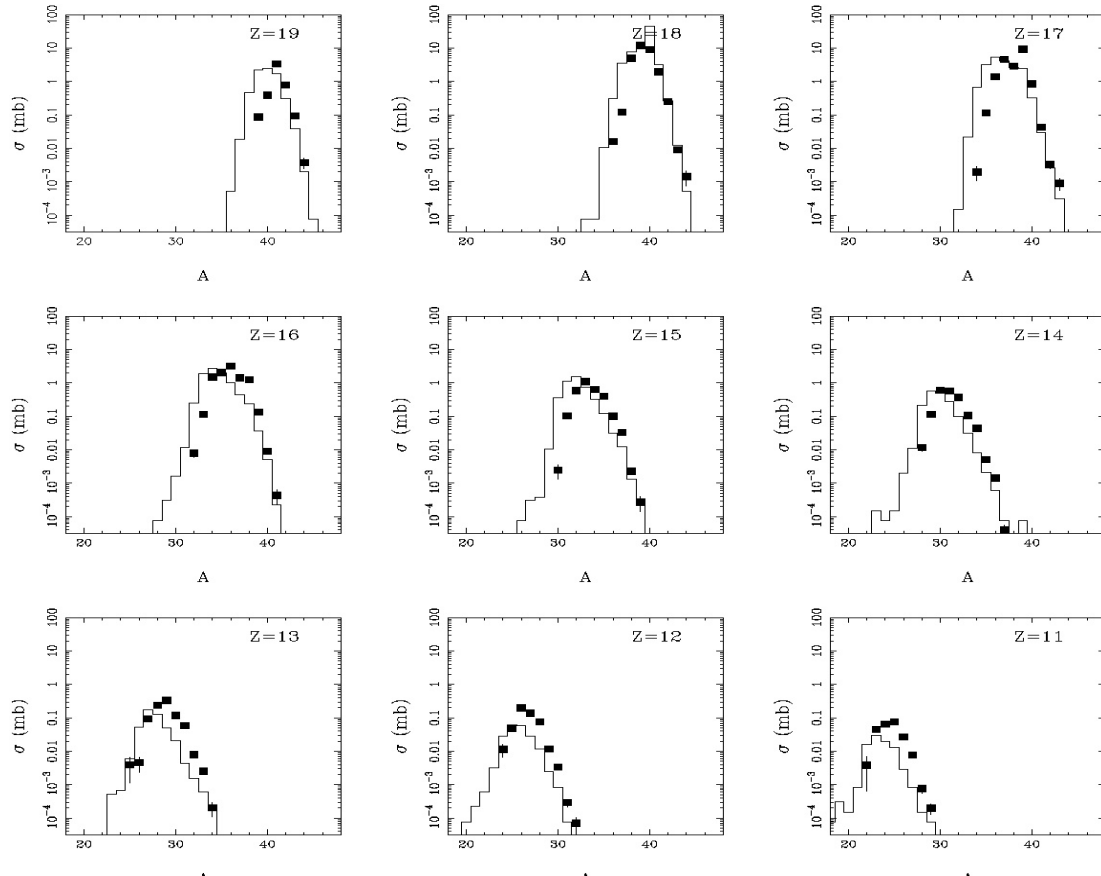**Figure 8**: Mass yield curves from the reaction ^{40}Ar+^{64}Ni at 15·A MeV at 4 degrees. Solid squares - measured data. Lines - result of the PE+DIT/ICF+SMM calculation [15,16,17], filtered by the spectrometer angular, azimuthal and momentum acceptance.

Figure 9 shows the results for the reaction ^{86}Kr+^{64}Ni at 15·A MeV, again at 4 degree setting. The products with Z=29-24 seem to be reproduced reasonably well by the PE+DIT/ICF+SMM simulation (pre-equilibrium emission followed by either deep-inelastic transfer or incomplete fusion followed by de-excitation using statistical model of multifragmentation).
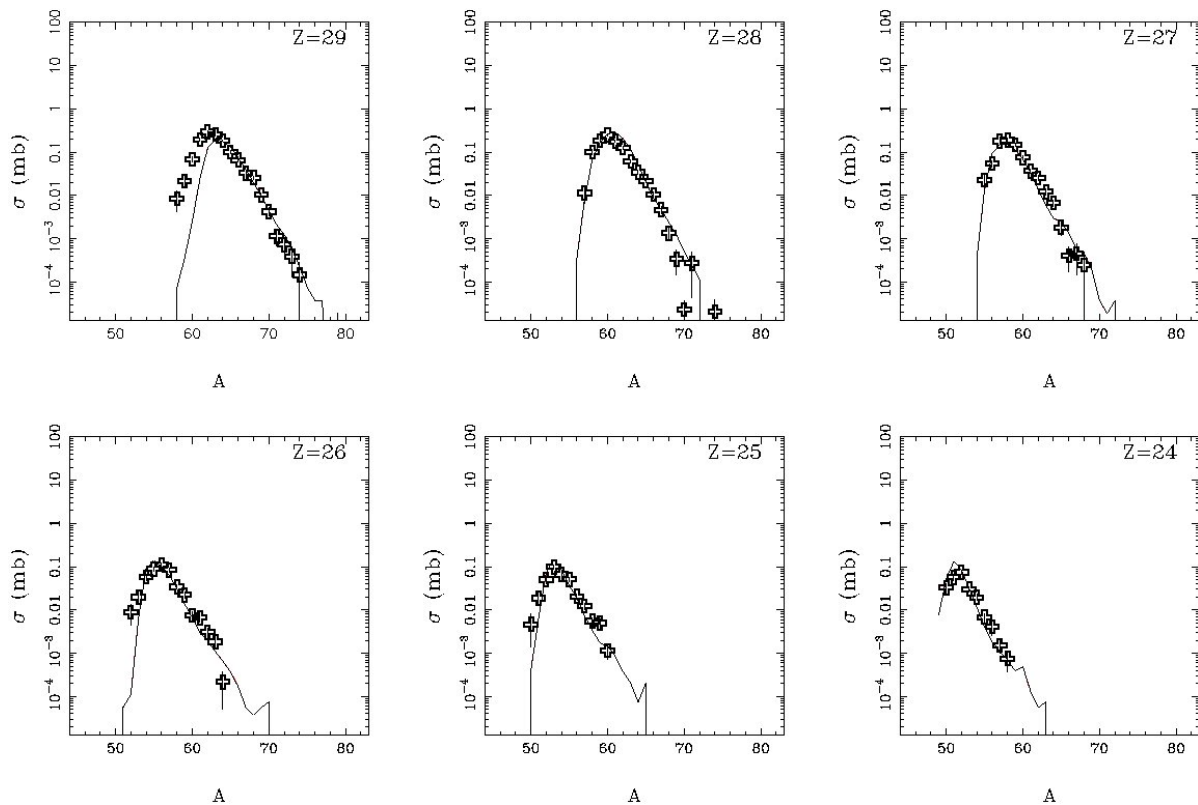
RIDS 515768	TASK: 11	DATE:	
DELIVERABLE: D2		PAGE 16	

Project funded by European Community under the "Structuring the European Research Area" Specific Programme Research Infrastructures Action within the 6th Framework Program (2002-2006)

Figure 9: Mass yield curves from the reaction [86]Kr+[64]Ni at 15·*A* MeV at 4 degrees. Symbols - measured data. Lines - result of the PE+DIT/ICF+SMM calculation [15,16,17], filtered by the spectrometer angular, azimuthal and momentum acceptance.

Figure 10 shows the comparison of the calculated total isotopic yields for the reaction [86]Kr+[64]Ni at beam energies 15·*A* MeV and 25·*A* MeV. It can be seen that the production cross sections do not drop during transition from 25·*A* MeV to 15·*A* MeV, the shapes of mass distributions remain similar, with some possible excess of neutron-rich nuclei appearing at 15·*A* MeV, representing a component produced mostly at higher angles, which thus needs verification in corresponding measurement since the present measurement does not provide direct answer.

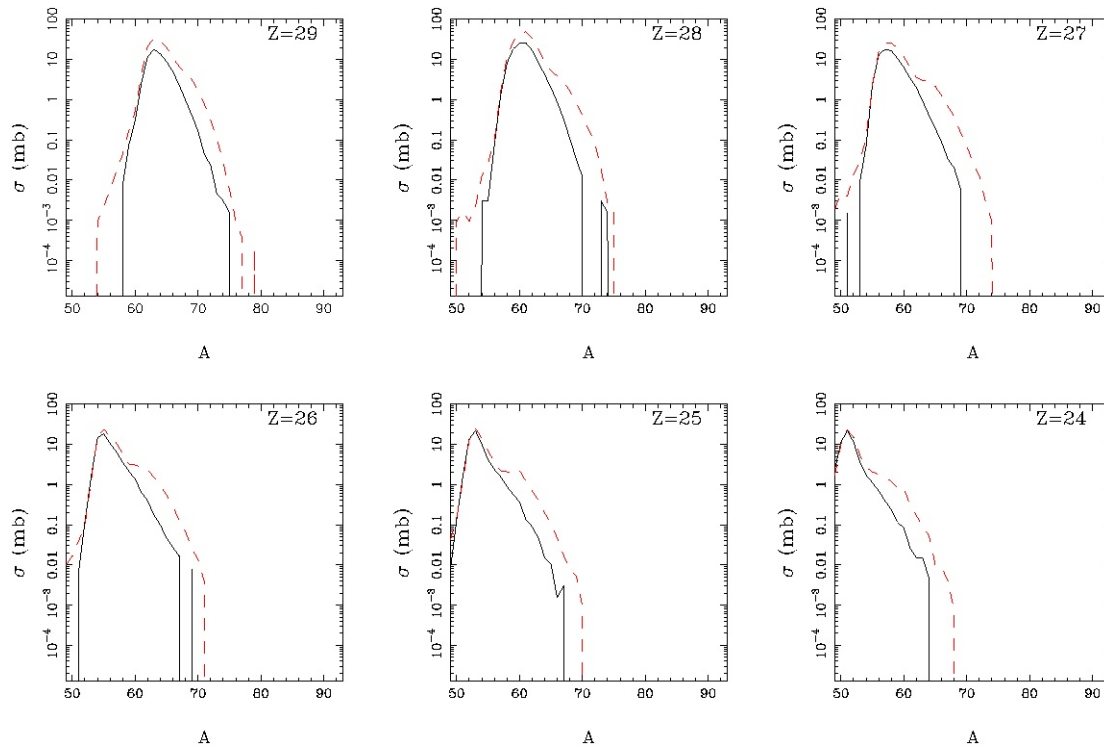| RIDS 515768 TASK: 11	DATE:	
DELIVERABLE: D2	PAGE 17	

Figure 10: Calculated total mass yield curves from the reaction ^{86}Kr+^{64}Ni at 25·*A* MeV (solid lines) and 15·*A* MeV (dashed lines).

I.2.3. Estimated yields

One of the promising ways to produce extremely neutron-rich nuclei around the neutron shell *N*=82 is fragmentation of a secondary beam of ^{132}Sn. Nevertheless, one can in principle consider also the reaction in the Fermi-energy domain at energies below 50·*A* MeV.

The in-target yields calculated using the production cross sections [17] are shown in Fig. 11. For the fragmentation of ^{132}Sn secondary beam an energy of about 100·*A* MeV was assumed. The achievable in-target reaction rate was determined using the code AMADEUS [19]. For the reaction ^{132}Sn+^{238}U at 28·*A* MeV a target thickness 40 mg/cm^2 was assumed. For the intensity of ^{132}Sn secondary beam a value of 10^{12} s^{-1} was adopted from Eurisol RTD Report. Due to larger target thickness, the in-target yield for fragmentation option calculated using the code COFRA [6] (dashed line), successful in reproduction of the secondary fragmentation experiment reported above, dominates for elements *Z*=44 and heavier, for lighter nuclei nevertheless the larger production cross sections in the Fermi-energy domain (solid line)

RIDS 515768	TASK: 11	DATE:	
DELIVERABLE: **D2**		PAGE 18	

Project funded by European Community under the "Structuring the European Research Area" Specific Programme Research Infrastructures Action within the 6th Framework Program (2002-2006)

leads to larger in-target yields despite relatively thin target and for Z=40 the in-target yield of extremely neutron-rich nuclei calculated using the PE+DIT/ICF+SMM appears to exceed the COFRA value. Thus, mainly due to possibility to transfer neutrons from the target to the projectile, at such extremely neutron-rich nuclei the Fermi energy option appears to be in principle competitive.
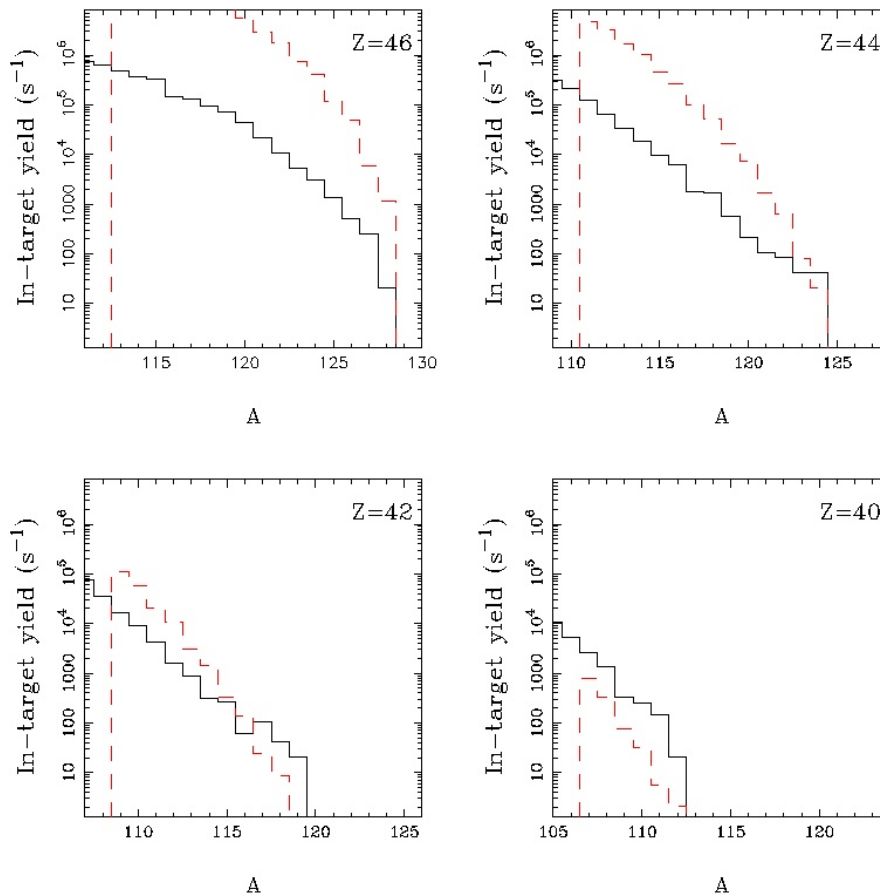

Figure 11: In-target yields calculated for the reaction $^{132}Sn+^{238}U$ at 28·A MeV (solid lines) and for the fragmentation of ^{132}Sn secondary beam an energy 100·A MeV (dashed line).

It however remains to be clarified what experimental equipment would assure that the yields of such nuclei could be collected and transported to the detection system. In the context of Eurisol post-accelerator, it appears as advisable to preserve maximum possible flexibility in available beam energies over the whole range from Coulomb barrier up to the maximum achievable energy.

RIDS 515768 TASK: 11	DATE:	
DELIVERABLE: D2	PAGE 19	

II Energy dependence of the charge-state distribution

The evolution of the ionic charge-state distribution as a function of energy is shown in Fig. 12 for $Z = 50$ and $Z = 30$. There are two problems connected with the charge-state distribution: One concerns the intensity, the other one the purity of the beam.

Since the fragment separator selects a nucleus in a specific charge state, the intensity of the wanted beam is proportional to the abundance of the selected charge state. From this criterion one could conclude that an energy of $60 \cdot A$ MeV is sufficient for obtaining about 50 % of the total intensity in the one-electron configuration. Higher abundances than 50 % in the completely stripped configuration are provided at energies above $80 \cdot A$ MeV.

The purity of the secondary beam after a magnetic selection is disturbed by contaminants of different ionic charge states. In particular when fragmentation products on the neutron-rich tail of the production are considered, less neutron-rich products, which are much more abundantly produced, pass the separator too. It depends on the requirements of the specific experiment, how much these contaminants disturb the experimental conditions. In view of the beam purity, an energy of at least $150 \cdot A$ MeV would be desirable.
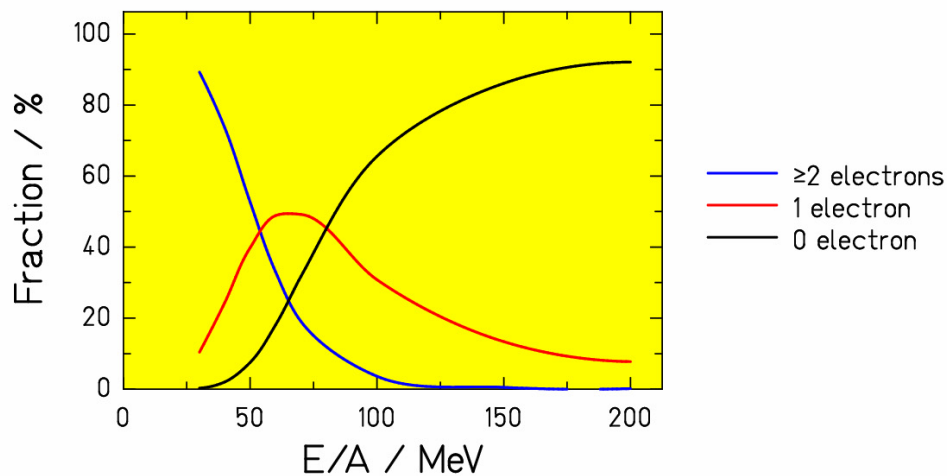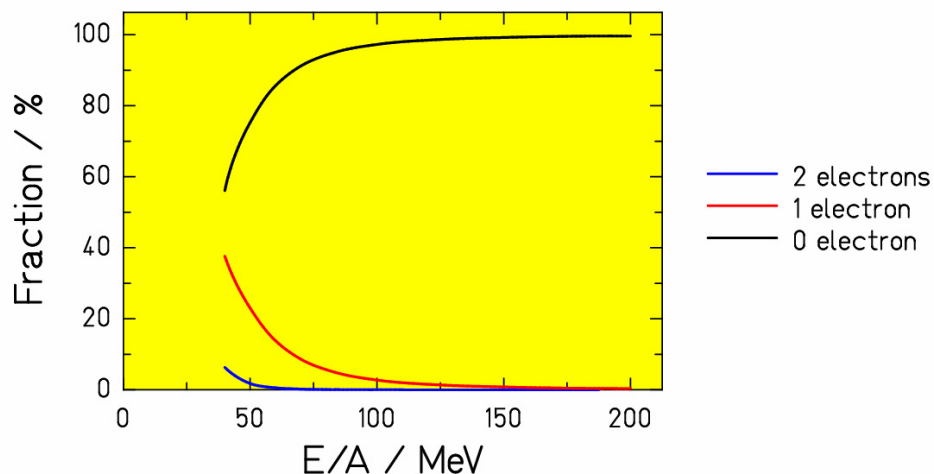
Figure 12: Charge-state probabilities of tin and zinc projectiles after a thick aluminium layer as a function of the energy.

III. Usable target thickness

There is a rather strict relation between the usable target thickness and the range of a projectile in the target medium for specific conditions on the emittance of the secondary beam. This relation is valid as long as the attenuation of the beam due to nuclear reactions in the target is negligible. In the case of 200·A MeV ^{132}Sn in beryllium, about 76 % of the projectiles are stopped by electronic interactions without

RIDS 515768	TASK: 11	DATE:	
DELIVERABLE: D2		PAGE 21	

Project funded by European Community under the "Structuring the European Research Area" Specific Programme Research Infrastructures Action within the 6th Framework Program (2002-2006)

From the numerical calculations presented in Fig. 13, one can extract that an energy increase by a factor of 2 leads to an enhanced total nuclear reaction rate by about a factor of 3.2.
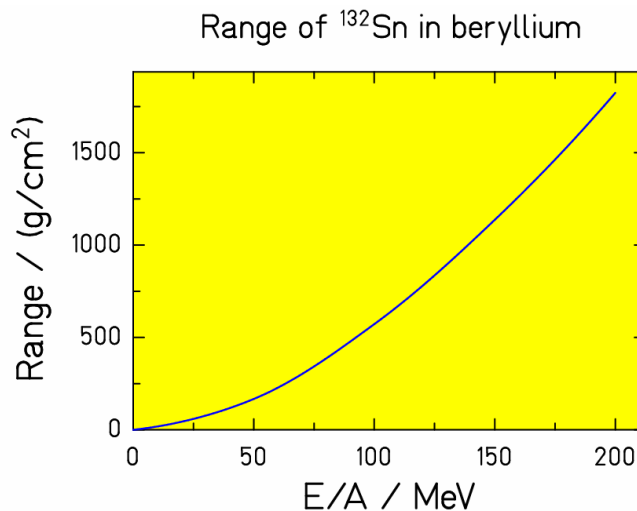

Figure 13: Range of ^{132}Sn projectiles in beryllium. The range increases by about a factor of 3.2 when the beam energy is doubled.

IV. Optimum post-accelerator energy

The optimum post-acceleration energy will be defined by the minimum value providing the largest produciton yield of exotic nuclei in fragmentation reactions but also giving access to the more diverse possible physics programme. From the point of view of the production it has been shown that the production cross sections of the most neutron-rich nuclei in fragmentation reactions do not depend on energy down to 150·A MeV. Therefore, the final yields will mostly depend on other arguments like charge-state distributions of the beam and residual nuclei and the usable target thickness.

A fraction of at least 50 % full stripped nuclei is obtained in the atomic energy range Z=30 to 50 for energies above 80·A MeV. However, if one requires a low fraction of contaminants in the beam this energy should be increased up to 150·A MeV. The usable target thickness is determined by the range on the projectiles in the target material and therefore by the projectile energy. In this respect the higher the

RIDS 515768	TASK: 11	DATE:	
DELIVERABLE: D2		PAGE 22	

energy the thicker the target that can be used taking into account that a factor of two in energy leads to a factor 3.2 increase in reaction rate.

All these arguments clearly justify as an optimum value for post-acceleration of 150·A MeV. Of course, this should be considered as a maximum value since lower energies would make possible the use of other reaction mechanisms like deep-inelastic reactions for the production of neutron-rich nuclei.

V. Summary

The results of the investigations performed under task 11.2 provide relevant arguments in favor of the Eurisol post-acceleration option. The specific experiment designed and performed in this task to investigate the fragmentation of neutron-rich fission residues, in particular ^{132}Sn, led to the following conclusions:

- The fragmentation of post-accelerated fission residues will completely filled the production gaps in ISOL-type facilities corresponding to refractory elements in the following atomic number ranges Z=40 to Z=45, Z=26 to Z=27 and Z=22 to Z=24.

- This option will also give access to extremely neutron-rich nuclei not reacheable to the single fission or spallation reactions taking place in ISOL facilities.

- These conclusions are valid for a post-acceleration energy as low as 150·A MeV.

Therefore the possibility of fragmenting fission residues post-accelerated around 150·A MeV would clearly contribute to significantly enlarge the nuclear landscape accesible to Eurisol. Indeed this option would offer a unique possibility for nuclear structure and nuclear astrophysics investigations with nuclei along the neutron shells N=50 and N=82. Reactions at lower energies could have some interest for the production of specific neutron-rich nuclei using transfer or deep-inelastic collisions.

The data obtained in this task concerning the yields of final nuclides produced in the fragmentation reactions of ^{132}Sn were compared to the ones obtained in other works on the fragmenation of the closest stable primary beam, ^{136}Xe, at a similar energy. This comparison yields that the production cross section of the most neutron rich nuclei along N=82 is around six orders of magnitude larger with the ^{132}Sn beam. Considering that the largest primary beam intensities expected in fragmentation facilities, e.g. FAIR or

RIDS 515768 TASK: 11	DATE:	
DELIVERABLE: D2	PAGE 23	

Project funded by European Community under the "Structuring the European Research Area" Specific Programme Research Infrastructures Action within the 6th Framework Program (2002-2006)

BigRIPS, is around 10^{12} ions s^{-1}, an expected intensity of post-accelerated fission residues at Eurisol around 10^{11} ions s^{-1} and a difference in target thickness of a factor of 10, still the post-acceleration option at Eurisol will produced yields of medium-mass neutron-rich nuclei four orders of magnitud more intense than in a fragmentation facility.

References

[1] K. Helariutta, J. Benlliure, M. V. Ricciardi, K.-H. Schmidt, Eur. Phys. J A 17 (2003) 181.

[2] H. Geissel, et al., Nucl. Instr. and Methods B 70 (1992) 286

[3] E. Casarejos, J. Benlliure, J. Pereira, et al., Phys. Rev. C 74 (2007) 044612

[4] J. Taieb, K.~H. Schmidt, L. Tassan-Got, et al., Nucl. Phys. A 724 (2003) 413

[5] P. Napolitani, et al., Phys. Rev. C 76 (2007) 064609

[6] J. Benlliure et al., Nucl. Phys. A 660 (1999) 87

[7] K. Summerer and B. Blank, Phys. Rev. C61 (2000) 034607

[8] J.-J. Gaimard, K.-H. Schmidt, Nucl. Phys. A 531 (1991) 709

[9] K.-H. Schmidt, et al., Phys. Lett. B 300 (1993) 313

[10] M. Caamaño, et al. Nucl. Phys. A 733 (2004) 187

[11] J. Benlliure et al., Eur. J. Phys. ST 150 (2007) 309

[12] J. Benlliure et al., Phys. Rev. C 78 (2008) 044616

[13] G.A. Souliotis et al., Phys. Lett. B 543 (2002) 163; G.A. Souliotis et al., Phys. Rev. Lett. 91 (2003) 022701.

[14] R.E. Tribble, R.H. Burch and C.A. Gagliardi, Nucl. Instr. and Meth. A285 (1989) 441; R.E. Tribble, C.A. Gagliardi and W. Liu, Nucl. Instr. and Meth. B56/57 (1991) 956.

[15] M. Veselsky, Nucl. Phys. A 705 (2002) 193.

[16] M. Veselsky, G.A. Souliotis, Nucl. Phys. A 765 (2006) 252.

[17] M. Veselsky, G.A. Souliotis, Nucl. Phys. A 781 (2007) 521.

[18] EURISOL Feasibility Study RTD, http://www.ganil.fr/eurisol/Final_Report.html

[19] Code Amadeus, http://www.gsi.de/charms/amadeus.htm